Combined Analytical/Numerical Modelling of Nucleation and Growth during Equiaxed Solidification under the influence of Thermal Convection

Wajira U. Mirihanage[1], David J. Browne[1]

[1]School of Electrical, Electronic and Mechanical Engineering,

University College Dublin, Belfield, Dublin 4, Ireland.

Abstract

Equiaxed grain solidification in inoculated melts is modelled on a macroscopic scale. The grain initiation is based on grain refiners present in the alloy melt as in most industrial castings. The Avrami analytical approach is used to model equiaxed growth. The model considers natural thermal convection and grain transportation by the resultant fluid flow. Flow characteristics during solidification are incorporated into the model by considering the equiaxed grains in undercooled liquid initially as slurry and later as a porous medium when it becomes coherent. Solidification of Al-7%wt.Si is simulated for different conditions. Evolution of cooling-curve characteristics are compared with a previous model and found to be in close agreement. The model simulation results suggest that nucleation can continue even after the recalescense. The limitation of grain refinement by recalescense and the potential influence of solutal effects are discussed. Simulated equiaxed grain size distribution and temperature evolution in the presence and absence of convention are compared and contrasted.

PACS : 64.70.-p; 05.70.Fh; 44.05.+e; 44.25.+f

Keywords: Equiaxed solidification , Convection, Grain transport

Nomenclature

C	- growth coefficient
C_p	- specific heat
D_l	- diffusivity of solute in the liquid
E	- source term account for latent heat
K	- permeability tensor
K_O	- morphological constant
L	- latent heat of fusion
N	- number of grains
S_x	-Source term to account for momentum modifications in horizontal direction
S_y	- Source term to account for momentum modifications in vertical direction
T	- temperature
V	- volume of grains
$\overline{V}^{old}$	- average envelope volume at the previous time step
$\overline{V}_{ex}$	- volume of previously nucleated (existing) equiaxed grains
$\overline{V}_{new}$	- envelope volume of newly nucleated grains
Z	- an increment of radius of the equiaxed mushy envelope
d	- grain diameter
f_s	- solid volume fraction
g	- gravitational acceleration
g_s	- solid fraction
k	- thermal conductivity
l_s	- solutal diffusion length
n_v	- number of seeds nucleated
p	- pressure
t	- time
u	- horizontal velocity
v	- vertical velocity
v_t	-dendrite tip velocity at current time
β	- expansion coefficient
$\varnothing$	- net equiaxed volume fraction of total grown envelopes
ΔS_v	- volumetric entropy of fusion
μ	- apparent viscosity
μ_0	- dynamic viscosity
ρ	- density
γ	- solid-liquid interfacial energy
η_{Ti}	- fraction of seeds initiated at undercooling ΔT_i
σ	- standard deviation
φ	- geometric mean

1.0 Introduction

Many engineering applications favour equiaxed grain structures in castings. Several models [1-7] have been proposed to describe the formation and growth of equiaxed grains. The early stage of equiaxed solidification was analysed in a model by Maxwell and Hellawell [1] which suggested that the number of grains is limited by recalescence during cooling. In Hunt's analytical model [2], the volume fraction of equiaxed grains was calculated using an extended volume concept, while liquid fraction within grains was calculated using the Scheil equation. Dustin and Kurz [3] used the concept of internal solid volume fraction of equiaxed grains, including features of grain number and recalescence. Considering solutal diffusion, Rappaz and Thevoz proposed numerical [4] and analytical [5] microscopic equiaxed solidification models at the scale of a single grain. Nucleation was assumed to occur at a single temperature. Following this, Wang and Beckerman [6] developed a model for equiaxed dendritic solidification, based on a multiphase approach and volume averaging. The model considered transport phenomena occurring on the system scale and grain nucleation and growth at microscopic scales. Solute transport was considered in the model. However, all of the models employed an instantaneous nucleation criterion, where nucleation occurs when the cited temperature of the liquid melt falls to a given nucleation temperature. However this is different from expected occurrences in real inoculated casting. Heringer et al. [8] and Gandin et al. [9] proposed one-dimensional isothermal models for equiaxed solidification. Both of these models were limited to one equiaxed grain and did not handle equiaxed nucleation in bulk liquid nor impingent and so are unsuitable for study of large alloy castings.

Greer et al. [7] developed a model for prediction of as-cast grain size in inoclulated melts. They modelled the appearance of grains controlled by the condition for free growth rather than by nucleation. The number of grains was limited by recalescence during cooling. The model by Quested and Greer [10] considered a log-normal distribution of inoculant particle size during nucleation and intended to establish the mechanisms that limit the number of grains in directional solidification. None of these models were extended to consider the influence of thermal convection and resultant fluid flow.

The main stimulus for current work is to develop a computationally efficient equiaxed zone model which can combine with the author's existing Front Tracking (FT) columnar zone model [11] to predict the Columnar to Equiaxed Transition (CET). The convective flow effects during the alloy solidification process are also to be treated. Basically this work bridges the macro-micro phenomena in equiaxed solidification. At microscopic scale it considers nucleation and growth and then average values are taken in to the macroscopic level representation, based on macro-scale conservation equations and flow characteristic evolution. The model predicts the nucleation, growth, impingement and transportation of equiaxed grains during solidification. Computations do not track the crystallographic or microscopic details for each dendrite, which reduces considerably the computational overhead. Complete casting simulations as detailed in the results section were executed within a few hours, on a personal computer. A non convective version of this model coupled with the FT columnar model was recently used for CET prediction. The simulated CET predictions found a good agreement with the experimental results [12]

As an initial research step, solute effects and sedimentation of equiaxed grains [13, 14] are not considered. However, solute effects are non-trivial for the grain sizes demonstrated in this work as discussed later. The main emphasis here is on natural thermal convention effects and resultant transport of equiaxed grains by fluid flow. Mesh sizes used in the simulations provide mesh size independent results and were chosen after a mesh refinement study.

2.0 Model

The following transient state conservation equations governing the transport of mass, momentum and energy in primitive variables are expressed in 2D as,

Energy,

$$\frac{\partial T}{\partial t} + \frac{\partial (uT)}{\partial x} + \frac{\partial (vT)}{\partial y} = \frac{k}{\rho C_p}\left[\frac{\partial^2 T}{\partial x^2} + \frac{\partial^2 T}{\partial y^2}\right] + E \qquad (1)$$

Momentum,

..in x – direction ;

$$\frac{\partial u}{\partial t} + \frac{\partial u^2}{\partial x} + \frac{\partial (uv)}{\partial y} = -\frac{1}{\rho}\frac{\partial p}{\partial x} + \frac{\mu}{\rho}\left[\frac{\partial^2 u}{\partial x^2} + \frac{\partial^2 u}{\partial y^2}\right] + (T - T_{ref})\beta g_x + S_x \qquad (2)$$

..in y – direction ;

$$\frac{\partial v}{\partial t} + \frac{\partial (uv)}{\partial x} + \frac{\partial v^2}{\partial y} = -\frac{1}{\rho}\frac{\partial p}{\partial y} + \frac{\mu}{\rho}\left[\frac{\partial^2 v}{\partial x^2} + \frac{\partial^2 v}{\partial y^2}\right] + (T - T_{ref})\beta g_y + S_y \qquad (3)$$

Continuity; on the assumption of liquid alloy as an incompressible fluid,

$$\frac{\partial u}{\partial x} + \frac{\partial v}{\partial y} = 0 \tag{4}$$

Where, u, v, T , t, p, μ, ρ, C_p, k and β are velocity in x direction, velocity in y direction, temperature, time, pressure, dynamic viscosity, density, specific heat, thermal conductivity and expansion coefficient respectively. S and E are source terms while g is external force (gravity) acting in x and y directions. The conservation equations are solved explicitly in a Cartesian fixed grid to obtain macroscopic temperature, node pressure, horizontal and vertical flow velocity for each time step.

2.1 Nucleation

Nucleation initiates from the seed particles (inoculants). This equiaxed crystal nucleation primarily depends on the seed particles' geometry as discussed by Greer et al. [7]. For free growth from an inoculation particle, the barrier to nucleation is overcome at the initiation undercooling, ΔT_i . which is a function of the diameter d, of the seed particle. The relationship is given by equation (5),

$$\Delta T_i = \frac{4\gamma}{\Delta S_v d} \tag{5}$$

Where ΔS_V is the volumetric entropy of fusion and γ is the solid-liquid interfacial energy.

Reaching the initiation undercooling is the condition required for free growth of the crystal from the seed particles [10]. Only one nucleation from any seed particle is possible. The probabilistic approach is used to calculate the number of nucleation sites activating at a given initiation undercooling.

This model considers the nucleation from inoculants with a given size distribution. As inputs, it requires distribution data of mean and standard deviation. If *f(s)* is the probability density function for distribution of seed particle diameter *s*, then the cumulative distribution function, *F(d)* for the same seed distribution could be defined as in equation (6); where *ds* is an infinitesimal diameter interval in the distribution;

$$F(d) = \int_0^d f(s)\,ds \tag{6}$$

This *F(d)* represents the fraction (probability) of seeds of diameter less than a given diameter, *d*. As indicated by equation (5) at some undercooling, ΔT_i , these small seeds have yet to be activated. So, therefore the fraction (probability), η_{Ti} of seed diameters above *d*, at such undercooling ΔT_i is,

$$\eta_{T_i} = 1 - F(d) \tag{7}$$

And the total number of possible nucleation sites, n_v for a given undercooling in any control volume (CV) is given by the product of: the seed density, $\omega_{i,j}$ (seeds per CV) and the fraction (probability), η_{Ti} of seed diameters above *d.* This relationship is expressed by,

$$n_v = \eta_{T_i}\ \omega_{i.j} \tag{8}$$

Hence, actual seed particle (inoculants) data with given size and density distributions can be used as modelling parameters. According to ref. [10], the size distribution of commercial innoculant particles used for aluminium alloy castings follows a log-normal distribution. Therefore, this model assumes the log-normal size distribution of inoculants and uniform density distribution throughout the casting. The probabilistic density function, *f(s)* used for a lognormal distribution is given by,

$$f(s) = \frac{1}{\sigma s\sqrt{2\pi}} \exp\left(-\frac{\ln s - \ln \varphi}{2\sigma^2}\right) \tag{9}$$

Where, σ and φ are related to the standard deviation and the geometric mean of the distribution. As undercooling increases new seeds are initiated, and the number of new initiations in each time step is given by the difference in the value of n_v between that at the current time and that at the previous time step, ie. ($n_v - n_v^{old}$).

2.2 Dendrite Growth

As in most previous models [eg. 2-4, 15], equiaxed grains are modelled as spherical in shape. In this model also, the hypothetical sphere that wraps around the dendrite tips is defined as a computational spherical equiaxed mushy envelope; which contains the inter-dendritic liquid and the solid dendrite. Growth of this envelope is computed using dendrite tip kinetics. The dendrite tip advancement or increment of radius of the equiaxed mushy envelope Z_t, in small time interval Δt, is given by,

$$Z_t = v_t\ \Delta t \tag{10}$$

Here, v_t dendrite tip velocity is calculated according to the Burden and Hunt [16] expression of dendrite tip kinetics. But it is quite possible to apply any other dendrite tip kinetic law [eg.17-19]. Following the Burden and Hunt kinetics; dendrite tip velocity v_t , at tip undercooling ΔT_t, is given by,

$$v_t = C\,\Delta T_t^2 \tag{11}$$

Here, C is the growth coefficient - an alloy dependent constant. For the 2D case, average mushy envelope volume (in 2D – actually this is area) of previously nucleated (existing) equiaxed grains, $\overline{V}_{ex}$ is calculated from the average envelope volume at the previous time step $\overline{V}^{old}$,

$$\overline{V}_{ex} = \pi\left(\left|\sqrt{\frac{\overline{V}^{old}}{\pi}}\right| + Z_t\right)^2 \tag{12.a}$$

Here, $\overline{V}$ (with cap) always denotes volumetric average values. The grain envelope size of just nucleated (new) equiaxed grain is given by,

$$\overline{V}_{new} = \pi Z_t^2 \tag{12.b}$$

At each time step nucleation and growth occur. The average size of all the nucleated envelopes in each CV is computed by averaging the diameters of newly nucleated envelopes and existing equiaxed mushy envelopes. The new total volume after each time step and starting average volume for next time step, $\overline{V}$ is given by,

$$V_{Total} = n_v^{old} \overline{V}_{ex} + (n_v - n_v^{old}) \overline{V}_{new} \quad (13)$$

$$\overline{V} = V_{Total} / n_v \quad (14)$$

2.3 Grain Impingement

At the early stage of solidification, equiaxed grains grow in relative isolation and move freely. When the equiaxed envelopes grow further, grains start to impinge upon each other. In this case, each time step is treated as isothermal and the extended volume concept [20] is used to calculate the net volume fraction of impinged equiaxed grains [2]. Net equiaxed volume fraction of total grown envelopes, ϕ over the complete solidification range is calculated using the relationship,

$$\phi = 1 - \exp\left[-\phi_{ext}\right] \quad (15)$$

Where, extended volume fraction ϕ_{ext} is given by,

$$\phi_{ext} = \frac{V_{Total}}{\Delta x \, \Delta y} \quad (16)$$

Then again, the true volume, $V_{i,j}$ of impinged grain envelopes in a particular CV (co-ordinates (i,j)) are recalculated according to,

$$V_{i,j} = \phi_{i,j} \, \Delta x \, \Delta y \quad (17)$$

where Δx and Δy are dimensions of a CV.

2.4 Solid Fraction Calculation

The solid fraction, g_s within the equiaxed mushy envelope is calculated via equation (18). The linear $g_s(T)$ relation is used for computational convenience.

$$g_s = \begin{cases} 0 & \forall \quad T \geq T_L \\ \dfrac{T_L - T}{T_L - T_S} & \forall \quad T_S < T < T_L \\ 1 & \forall \quad T \leq T_S \end{cases} \tag{18}$$

And the solid volume fraction in any CV, f_s is given by,

$$f_s = g_s \left(\frac{V_{i,j}}{\Delta x \, \Delta y} \right) \tag{19}$$

Other non-linear $g_s(T)$ relationships can also be used with the model. e.g. from the Scheil equation[21]. Simulations were carried out by the authors using such a relationship, but minimal change in the predictions of the model were observed and therefore the simplified linear relationship was maintained in the model as it obviates the need for a numerical iteration process in the calculations.

2.5 Grain Transport

The liquid metal co-existing with initially free equiaxed grains is considered via a model of slurry. The transportation of nucleated equiaxed grains with fluid flow is demonstrated with the simplified assumption considering the system as a solid–liquid suspension. It is assumed that grains move with velocity equal to that of the flow

within the fluid. As a result of the liquid flow, the number of grains and equiaxed grain volumes in any CV are continually changing and this in addition to the effects of nucleation and growth. The number of grains N, is different to the number of nucleated grains, n_v in the CV.

Only at the beginning for the first nucleation event,

$$N_{i,j} = n_{v_{i,j}} \qquad (20.a)$$

Then with nucleation and flow,

$$N_{i,j}^{new} = N_{i,j} + \frac{1}{\Delta x \Delta y} \left[\pm N_n \left| v_{i,j+1} \right| \Delta x. \pm N_s \left| v_{i,j} \right| \Delta x \pm \ldots . \right.$$

$$\left. \ldots . N_e \left| u_{i+1,j} \right| \Delta y \pm N_w \left| u_{i,j} \right| \Delta y. \right] \bar{\Delta} t \qquad (20.b)$$

In equation (20.b), ± represent the appropriate use of direction of flow (in/out of a CV) with the magnitude of the flow velocity. N_n , N_s , N_e and N_w represent the number of nucleated grains in given neighbouring CVs according to the flow directions in all four sides as in figure 1 and subscripts *n, s, e, w* refers to neighbouring CVs to the north, south, east, west respectively as commonly use in control volume methods.

The number of grains in a CV changes due to two separate phenomena during a single time step; by new grain initiation and due to the flow effects. Similarly, the net resultant mushy envelope volume also changes from the transportation from/to neighbouring CVs at particular time given by,

$$V_{i,j}^{new} = V_{i,j} + \frac{1}{\Delta x \Delta y} \left[\pm V_n \left| v_{i,j+1} \right| \Delta x \pm V_s \left| v_{i,j} \right| \Delta x \pm .... \right.$$

$$\left. .... V_e \left| u_{i+1,j} \right| \Delta y \pm V_w \left| u_{i,j} \right| \Delta y \right] \Delta t \qquad (21)$$

Hear all the nomenclature is the same as for equation (20) and V_n , V_s , V_e and V_w represent the equiaxed volumes in neighbouring CVs matched to the flow directions on all four sides as in figure 1.

2.6 Flow Characteristics

At low equiaxed solid volume fractions, the equiaxed region is modelled as a slurry. For such a slurry, viscosity is a function of the volume fraction of solid, f_s; and the modified viscosity, μ, is obtained using the Thomas' empirical approximation cited in ref.[22] and is given as,

$$\mu = \mu_0 \left[1 + 2.5 f_s + 10.05 f_s^2 + A \exp(B f_s) \right] \qquad (22)$$

Where; μ_0 is viscosity of the pure liquid phase of the alloy and A and B are constants. This method is based on the replacement of the physical viscosity with an effective viscosity that can increase with solid volume fraction.

When higher solid volume fraction has developed the flow of equiaxed mush in the undercooled zone is no longer possible model as a slurry (liquid-solid suspension) only. A coherent equiaxed dendrite network produces the environment similar to typical porous medium. Therefore, after the local solid volume fraction, f_s exceeds the

coherency fraction, f_{coh} , the local domain is considered as a porous medium [23]. With the growth of the volumetric solid fraction, the resultant internal flow resistance is growing in the undercooled liquid. According to the Darcy law, velocity extinction is taken into consideration by using the source terms S_x and S_y in the momentum equations (2) and (3) [24, 25].

For such systems, and with the assumptions of stationary solid phase, the phase interaction forces are proportional to the artificial liquid velocity. The source terms S_x and S_y are given by ref.[24] as,

$$S_x = -\frac{\mu_0}{\rho} K \bar{u} \tag{23}$$

$$S_y = -\frac{\mu_0}{\rho} K \bar{v} \tag{24}$$

Where, K is the permeability tensor - physical property of a porous medium, which specifies the medium resistance to the flow. Anisotropy of flow conditions in the mushy zone comes from strongly directional nature of dendrite growth. However, it is a common practice to simplify equations (23) and (24) by the assumption that the mush is isotropic [23, 26]. Therefore, the permeability tensor K is defined by Blake-Carman-Kozeny model using morphological constant K_O as,

$$K = K_O \frac{f_s^{\,2}}{(1 - f_s)^3} \tag{25}$$

and is considered a scalar quantity here.

2.7 Latent Heat Evolution

Latent heat effects are incorporated into the model via the source term *E* in equation (1). The contributions to temperature change by latent heat come from changes of mushy envelope volume as well as change of solid fraction within each envelope over the time [11]. The mathematical relationship for absorbed /released latent heat is given according to,

$$E = \frac{L}{C_p}\left[f_s \frac{\partial V}{\partial t} + V \frac{\partial f_s}{\partial t} \right] \quad (26)$$

where *L* is latent heat of fusion. Results of these changes include the latent heat release as well as absorption of latent heat of fusion. The heat releases are visible in equiaxed grain solidification. Absorption of heat of fusion occurs during re-melting of the solidified grains when transported to the superheated liquid regions by fluid flow.

3.0 Results

Model simulations were carried out considering different scenarios. Liquid melt with inoculants was considered and it was assumed that no columnar growth occurred. Al-7%wt.Si was taken as the considered alloy for all cases. Aluminum and silicon have similar densities, so solutal convection can be easily ignored. A rectangular mould casting (height-‘*y’ direction* and width-‘*x’ direction*) was taken with the assumption that the front and back faces are fully insulated and hence adiabatic. This brings zero heat flux along the perpendicular direction (‘*z’);* which converts the system to 2D. The following thermo-physical properties of the alloy and other

parameters are common to all simulations ; $L = 400\ kJkg^{-1}$, $k=100\ Wm^{-1}K^{-1}$, $\rho=2600\ kgm^{-3}$, $C_p= 1000\ kgK^{-1}$, $h=3000\ Wm^{-2}K^{-1}$, $\mu_0=1.3X10^{-3}\ kgm^{-1}s^{-1}$, $\beta= 7.1X10^{-4}\ K^{-1}$, $C=5.0X10^{-6}\ K^2m^{-1}s$, $K_0= 4.92X10^{7}\ m^{-1}$, $T_L=891\ K$, $T_S=850\ K$, $g_x= 0.0\ ms^{-2}$, $g_y= 9.81\ ms^{-2}$ and $f_{coh}= 0.6$.

The value of f_{coh} of 0.6 was taken as the upper limit for dendrite coherency from ref. [22]. However other researchers [27-29] have suggested lower values for aluminium alloys. This is discussed later (in Section 4).

3.1 Initial Stage of Solidification with Single Inoculants Size

Initially, simulations were performed for isothermal like cooling (cooling with very low thermal gradient with in the sample) of small *0.05m X 0.05m* sample from the liquid phase. A mixed boundary conditions control heat extraction from the domain. For this simulation, nucleation particles with the exact size of *0.65μm* were chosen without any size distribution (standard deviation of zero). So, all of the available nucleation seeds were starting to activate instantaneously. Initial portions of the cooling curves for different numbers of seed particles are presented in figure 2. Curves labelled ***A – E*** represent the simulated cooling curves obtained with different numbers of nucleation seeds (*25, 75, 125, 200 and 300* respectively); which result different grain sizes. Curve ***A*** relates to a final average grain diameter of 11.3mm. curves ***B, C, D*** and ***E*** relate to final grain diameters of *6.5mm, 5.0mm, 4.0mm* and *3.3 mm* respectively.

3.2 Inoculants with Size Distribution

Simulation was again carried out for *0.05m X 0.05m* casting size. Again here also mixed boundary conditions control heat extraction from the domain; the entire domain

was modelled isothermally to prevent any effects from heat diffusion or convection and also made system simple and easy to study. In this simulation, nucleation seed particle sizes were scattered and not uniform, size distribution following the log-normal distribution as in typical industrial TiB_2 inoculants [10]. The model simulation results are summarized in figure 3. Temperature is presented by the thick line; the thin line gives the fraction of activated nucleation particles. Local equiaxed volume fraction is given by the dotted line.

3.3 Full Casting Simulations

Complete solidification simulations were performed for Al-7%Si casting; considering a rectangular mould casting of a size of *0.2m X 0.2m* (height-'*y' direction* and width-'*x' direction*). Initial pouring temperature was set with *5K* super heat (*896K).* Imposed flow after pouring was assumed as zero. The mould temperature was set to *725K* constant. The total number of inoculant particles in the melt was set to *5,000*. Initial simulation was performed with the presence of convective heat transfer and equiaxed grain transportation due to flow. The simulation was repeated, the only difference being the setting of external force (gravity) to zero *(g=0).*

The simulated temperature profiles are shown in figure 4. The profiles were simulated for the scenarios in the presence of convective flow and in the absence of convection. The figure numbers *a1, a2* and *a3* show temperature profiles at *30, 50* and *70* seconds after pouring respectively with convection, whereas *b1, b2* and *b3* shows profiles for the same times but without the effects of convection. Figure 5 show the simulated cooling curves during solidification. In figure 5, curve '***a***', is close to the outer part of the sample while curve '***b***' is from a point between the outside and the centre of the

sample (curve '***c'***). Thin continuous lines were from the simulation with convective effects and thick dotted lines were from the simulation without convection. The locations of points ***a, b*** and ***c*** are marked in figure 6. Figure 6.A presents the contour plot of equiaxed grain sizes from simulation with thermal convection and grain transportation while figure 6.B presents the contour plot of equiaxed grain sizes when no external force(gravity) acts.

4.0 Discussion

According to Flood and Hunt [15], there are two basic requirements for formation of an equiaxed zone.

(i) The presence of active nuclei

(ii) Favourable conditions promoting their growth

The presence of inoculants in the undercooled liquid satisfies both of these requirements. Here we concentrate only on equiaxed nucleation in the presence of purposely added inoculants and no effort has been made to consider other nucleation sources such as nucleation from tip fragmentations or impurities etc..

For numerical simulations, the conservation equations were solved using an explicit method. Due to the very small time step needed for stability of the solution using the explicit method this could be viewed as a disadvantage. However, complexity and nature of the problem demand high temporal resolution; larger time steps may not be able to compute a smooth continuity of grain growth and related developments correctly. So in this case, the use of an explicit scheme is not a disadvantage for numerical computational efficiency.

As a preliminary study, the initial influence of grain density on equiaxed grain growth was performed and isothermal samples were considered. As detailed in figure 2, with increasing grain density (resulting in decreasing final grain diameter) recalescence starts at higher temperature and the recalescence region becomes narrow. Thus, equiaxed grain growth rates are lower in this region due to low undercooling. These results are in qualitative agreement with the results from the solute diffusion model of Rappaz and Thevoz [4, 5] and also with the experimental results of Al-7%Si alloy presented in the same publication.

Grain initiations from seed particles with a range of sizes were then simulated. In this simulation convection and resultant grain transportation was switched off for simplicity. Here, T_L for the alloy is *891K* and as soon as the temperature drops below T_L nucleation seeds started to activate. Larger particles start grain initiation initially; then followed by increments of descending diameter with decreasing temperature (increasing undercooling). As shown in figure 3, until the temperature reaches a minimum before recalescence (***q***), more and more seeds were continuously activated. After reaching the point ***'q'***, the local temperature started to rise as a result of the release of latent heat. Shortly after this the temperature decreased to the previous minimum level (at '***r'***) before further decrease. During this interval, the plateau (***p – s***) in the nucleation curve shows no new grain initiations. Therefore at this point, initiation was clearly controlled by the recalescence. However, after the temperature reaches point '***r***' of the temperature curve, grain initiation resumes again - as seen in figure 3. This is quite possible, provided the equiaxed volume does not fully occupy the undercooled liquid. During the recalescence, equiaxed grain volume increases to

occupy considerable fraction of the undercooled melt but some unoccupied liquid area (volume in 3D) still remains as space for grain initiation. Therefore, grains could still be initiated even after the recalescence. But results also show that the maximum initiation undercooling was not enough to start grain initiation from all the nucleation seeds before the undercooled liquid was fully occupied by equiaxed mush. Another interpretation is that all inoculants of a size greater than that relating (via equation (5)) to the undercooling at *'q'*(on the cooling curve) would have been activated by the relevant time. As temperature then increases, the reduced undercooling means that no further nucleation is possible. It is only after the temperature reaches that at *'q'* again (*'r'* on cooling curve) that increased undercooling allows nucleation process via activation of the smaller seed particles.

In this model the undercooling level is determined from the constant T_L, which does not consider the possibility of solute enrichment of remaining liquid metal due to solute rejection from the growing solid. Such solute enrichment could move the undercooled liquid composition to right, in phase diagram (position from '***p1***' to '***p2***' as in the figure 7). Such a shift of composition would reduce the actual undercooling (as $\Delta T_2 < \Delta T_1$ in fig. 7). Under such conditions we would have lower actual undercooling; new nucleation initiations from smaller inoculants would have even less chance to occur before the undercooled melt becomes fully occupied by the growth ie. grain initiation could be completely halted. However in systems where solute enrichment during undercooling is negligible there is still possibility of new nucleation even after the recalescence. Extra-dendretic solute enrichment of bulk liquid can generally be neglected in diffusion controlled growth, although it can be significant if the morphology of the growing primary phase is globular as opposed to

dendretic [30]. Therefore, recalescence is not a completely limiting factor for the refinement of grain size. Restating of grain initiation after recalescence is like to be very much dependant on solute enrichment.

In these simulations, the numbers of inoculants was restrained to maintain the final equiaxed grain size in the millimetre range. That keeps the separation distance greater than the solutal diffusion lengths during the growth (except for negligible shorter period before impingement). This enables justification here of the non-consideration of solutal effects. As shown in [31], it is possible to ignore the solutal effects when separation distances of the grains are greater than to the solutal diffusion length. According to [32] an estimate for the solutal diffusion length, l_s is given by,

$$l_s = \frac{D_l}{v_t} \tag{27}$$

where, D_l is the diffusivity of solute in the liquid and v_t, is velocity of the dendrite tip equal here to that of the grain envelope. The mean solutal length for both cases (terrestrial and zero-g) remains at the maximum level of $80\mu m$ (when, $D_l=6.4X10^{-9}$ m^2s^{-1}). This is reasonably small compared to the possible separation distances of equiaxed grains, which has average final size of *3.72mm*; ranging from *3.48 mm* to *3.95 mm* in the simulation with convective affects. Further research is in progress to integrate grain sedimentation and solute effects to the model presented here to enable improved predictions for much smaller grain sizes.

The solidification simulation with gravity as external force in the *'y'* direction, simulates the resultant thermal natural convection and grain transportation by flow, as in normal industrial casting. The zero external force results in no convectional effect which resembles solidification under microgravity. The temperature profiles from all the simulations showed vertical symmetry [33], whether convection was present or not. At the same time, simulation results with no convection shows four fold symmetry over both vertical and horizontal centre axis.

These simulations use f_{coh}=0.6 - it is the upper limit on values given in ref. [23]. Other work [27-29] suggests much lower values for f_{coh}. However, according to Chai et al. [34] "smaller grain sizes correspond to a shorter distance between grains, which tend to make the dendrites become coherent earlier". The suggested f_{coh} values given in the previous literature [27,28] were found using grain sizes much smaller (within a range below 1mm) than those demonstrated in the current simulations (in the range of 3 - 4mm). Therefore, the upper limits of experimental values [23] are used in the simulation. However, the authors have not found a large sensitivity of the model predictions to the value of the f_{coh} used.

As in most industrial casings, fine grains close to the mould wall and course grains in centre portion are apparent from figure 6. As with the temperature profiles, simulated grain size contours also show only two fold symmetry in the presence of convective effects, but when convective heat transfer and grain transportation are not present it becomes four fold symmetry. In convective and non-convective simulations, approximately *3740* and *3700* total grain initiations occurred, respectively. Relatively quick cooling due to convection may cause the slightly higher number of equiaxed

grain initiations. This initiated figure is around two thirds of the total nucleation particles which were used (*5,000*). The remaining smaller nucleation particles are unable to nucleate at the local under-cooling available before the undercooled liquid becomes occupied due to growth. However after the completion of solidification, approximately *3670* equiaxed grains remained in the simulation with convective effects and all the initiated *3700* equiaxed grains remained in the simulation without convection. The disappearance of some initiated grains was due to the re-melting of those that were transported into superheated liquid by the fluid flow. According to the simulation results, this figure is around *2* percent, which is actually not sufficient to alter the average grain size significantly. But, much larger mould dimensions and steeper temperature gradients may cause higher convective effects resulting in much higher re-melting rates of initiated equiaxed grains which could lead to significant alterations of the outcome. The instantaneous dissolving of such grains was assumed in the model. However, in reality they could survive for a certain time period and could lead to grain formation again, as discussed in ref. [35].

5.0 Conclusion

An equiaxed solidification model in 2D is proposed and simulations were performed for an Al-7%wt.Si alloy. Simulations show characteristic equiaxed cooling-curves including recalesences during the initial solidification period. Recalesence patterns for different nucleation density causing different final grain sizes were found to be in good qualitative agreement with previous modelling attempts and experimental results in the literature. The simulations show there are new grain initiation possibilities even after recalesence but depending on solute effects. Hence recalecences are not always a

severe limiting factor for grain refinement. This model is limited to the growth scenarios where solutal diffusion lengths are reasonably smaller than the equiaxed grain sizes. Model simulation predicts four fold symmetric grain size distribution in a square mould for microgravity conditions, where thermal convection and equiaxed grain transportation is absent. When convective affects are present, equiaxed grain size distribution is altered and no longer shows four fold symmetry in the square mould.

6.0 Acknowledgement

The authors wish to acknowledge the financial support of European Space Agency (ESA) under the PRODEX program, (contract number 90267). This work is part of the ESA-MAP (Microgravity Applications Project) project CETSOL.

7.0 References

[1] Maxwell I., Hellawell A., Acta metal., 1975, Vol. 23, pp. 229-237

[2] Hunt J.D., Mater. Sci. Eng., 1984, Vol. 65, pp. 75-83

[3] Dustin I., Kurz W., Z. Metallkd., 1986, Vol. 77, pp. 265-263

[4] Rappaz M., Thevoz Ph., Acta Metall., 1987, Vol. 35, pp. 1487-1497

[5] Rappaz M., Thevoz Ph., Acta Metall., 1987, Vol. 35, pp. 2929-2933

[6] Wang C.Y., Beckermann C., Metal. Mater. Trans. A, 1996, Vol. 27, pp. 2754-2763

[7] Greer A.L., Bunn A.M, Tronche A., Evans P.V., Bristow D.J., Acta Mater., 2000, Vol. 48, pp 2823–2835

[8] Heringer R., Gandin Ch. A., Lesoult G., Henein H, Acta Mater., 2006, Vol. 54, pp. 4427-4440

[9] Gandin Ch. A., Mosbah S., Volkmann Th., Herlach D.M., Acta Mater, 2008, Vol. 56, pp. 3023-3035

[10] Quested T.E., Greer A.L., Acta Mater., 2005, Vol. 53, pp 4643-4653

[11] Browne D.J., Hunt J.D., Num. Heat. Trans. B, 2004, Vol. 45, pp 395-419

[12] Mirihanage W.U., McFadden S., Browne D.J., "A New Macroscopic Model for Prediction of Columnar to Equiaxed Transition using Front Tracking" (Paper presented at 5th International Conference on Solidification and Gravity, Miskolc-Hungary, 3rd Sep. 2008), p.63

[13] Lesoult G., Mater. Sci. Eng .A, 2005 , Vol. 413, pp.19–29

[14] Geo J. Y. and Wang C.Y., Trans. ASME, 1999, Vol. 121, pp. 430-437

[15] Flood S.C., Hunt J.D., J. Cryst. Growth, 1987, Vol. 82, pp 552-560

[16] Burden M.H., Hunt J.D., J. Cryst. Growth, 1974, 22, pp 109-116

[17] Hunt J.D., Lu S.-Z., Metall. Mater. Trans. A, 1996, Vol. 27, pp. 611-623

[18] Lipton J., Glicksmam M.E., Kurz W., Mater Sci. Eng., 1984, Vol. 65, pp. 57-63

[19] Kurz W., Gioranola B., Trivedi R., Acta Metall., 1986, Vol. 34, pp. 823-829

[20] Christian J.W., Theory of Transformations in Metals and Alloys, Pergamon, Oxford, 1975, p 17

[21] E. Scheil. Bemerkungen zur schichtkristallbildung. Zeitschrift fur Metallkunde, 1942, 34:, pp.70–72

[22] Qin R.S., Fan Z, Matter. Sci. Technol. ., 2001, Vol. 17, pp1149-1152

[23] Ilegbusi O.J., Mat M.D., Mater. Sci. Eng. A, 1998, Vol. 247, pp. 135-141

[24] Brent A.D., Voller V.R., Reid, K.J, 1988, Num. Heat Trans. 13, pp 297-318

[25] Swaminathan C.R., Voller V.R., Metall.Trans.B,1992, Vol 23, pp.651-664

[26] Banaszek J, McFadden S., Browne D.J., Sturz L., Zimmermann G., Metal. Mater. Trans. A.., 2007, Vol. 38A, pp 1476-1484

[27] Veldman N. L. M., Dahle A. K.,. StJohn D. H., Arnberg L., Metallurgical and Materials Transactions A, 2002, 32A, pp.147-155

[28] Dahle AK, Arnberg L. Rheological properties of solidifying aluminium foundry alloys. 1996, JOM;March

[29] Brabazon D., Browne D.J., Carr A.J., Mater. Sci. Eng. A., 2003, vol. A356, pp. 69-80

[30] Martorano M.A., Beckermann C., Gandin Ch-A., Metall. Mater. Trans. A; 2003, vol 34A, pp 1657-1674

[31] McFadden S., Browne D.J., Scripta Mater., 2006, 55, pp 847-850

[32] Rappaz M., Boettinger W.J., Acta. Mater, 1999, Vol. 47, pp. 3205-3219

[33] McFadden S., Sturz L., Jung H., Mangelinck-Noel N, Nguyen_Thi H., Zimmermann G., Billia B., Browne D., Voss D., Jarvis D.J., J. Of the Japan Society of Microgravity Applications, 2008, Vol 25:No.3, pp.489-494

[34] Chai G., Backerud L., Rolland T., Arnberg L., Meal Mater. Trans. A., 1995, vol 26A, pp.965-970

[35] Han Q., Hellawell A., Metall. Mater. Trans. B, 1997

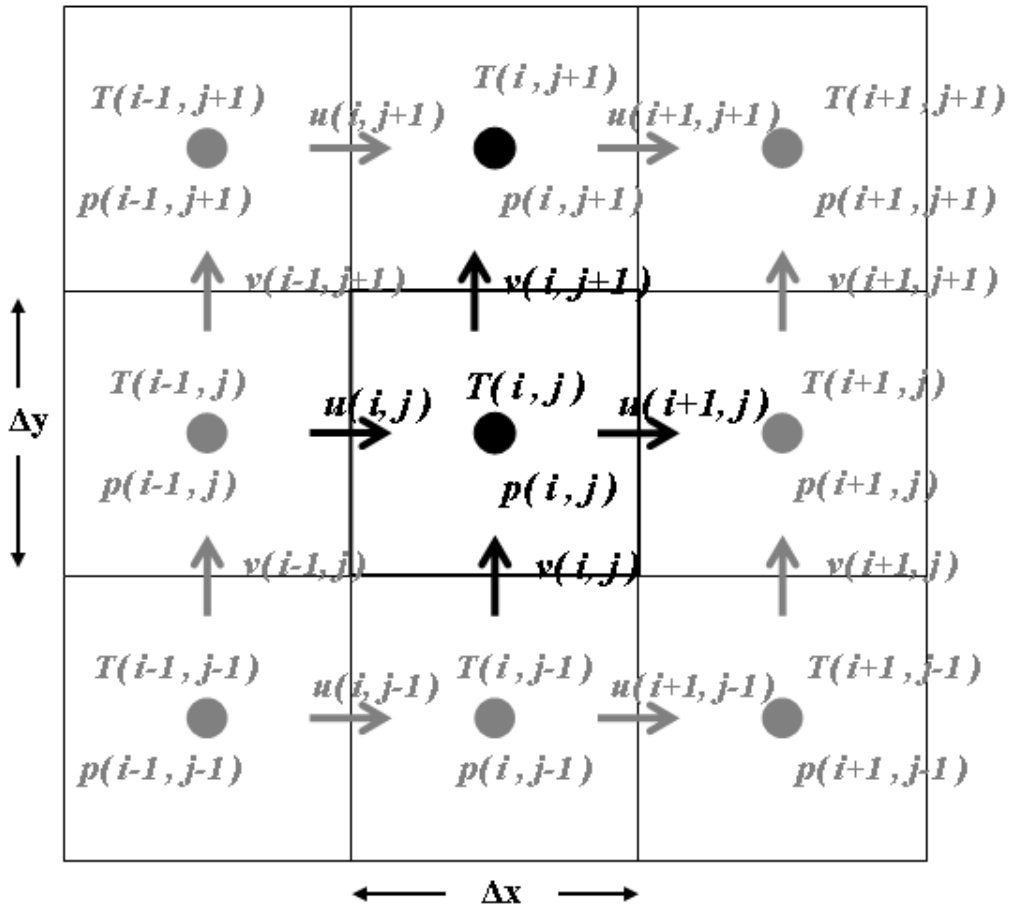

Figure 1. Node and flow notation

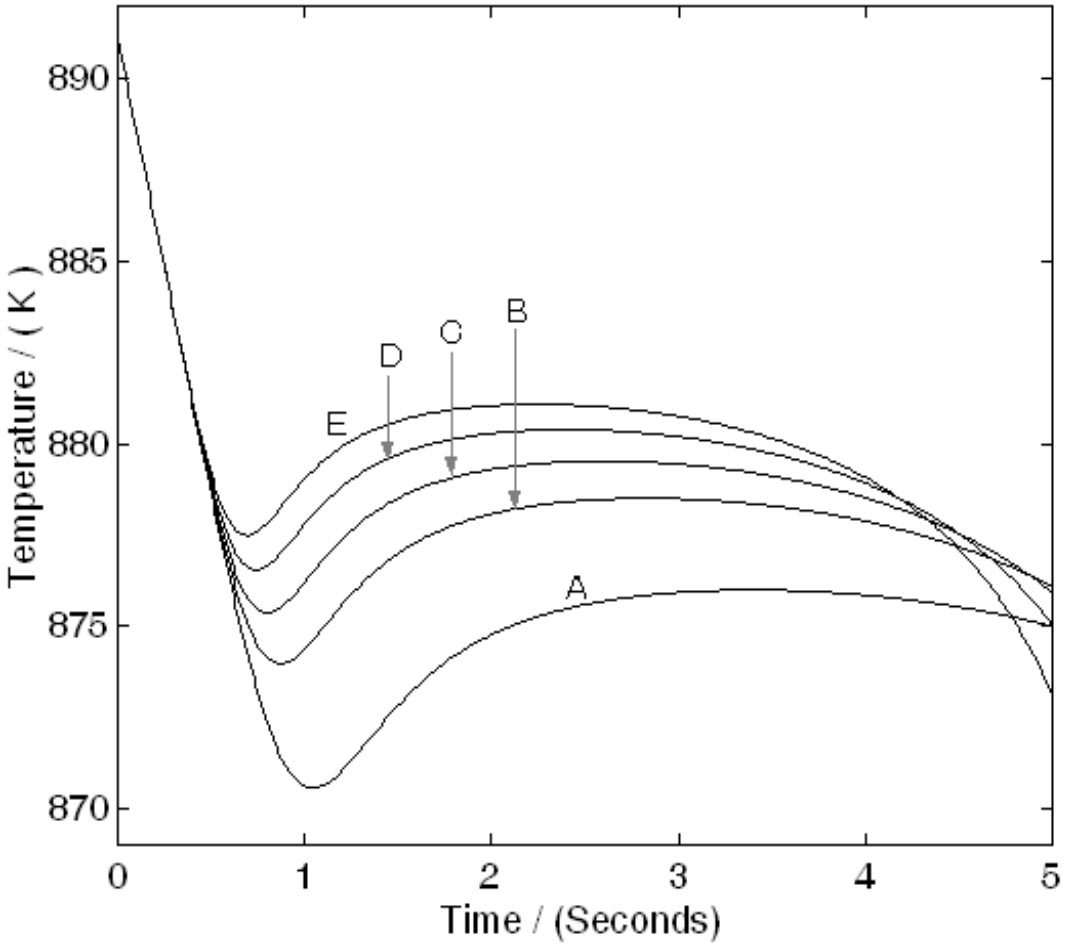

Figure 2. Recalescence in cooling curves for various number of nucleation seeds A- 25 seeds, B-75 seeds, C-125 seeds, D-200 seeds and E-300 seeds

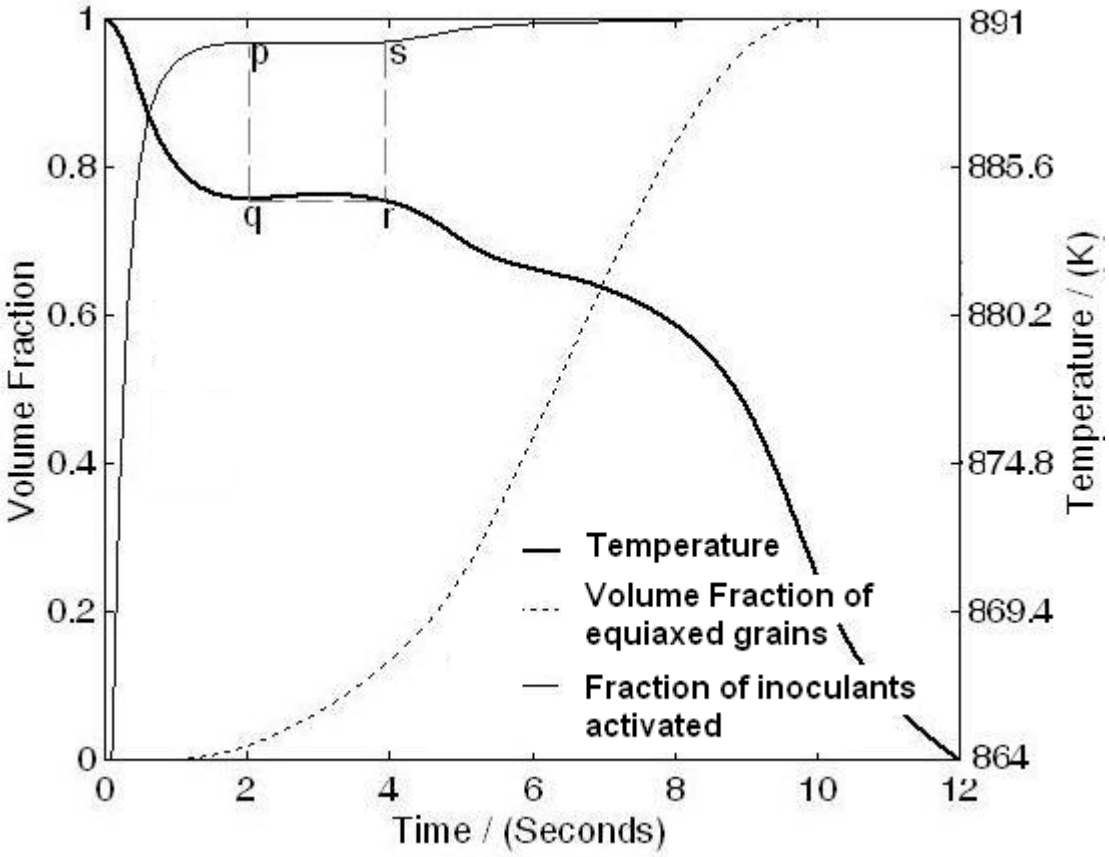

Figure 3. Simulated cooling curve (thick line) fraction of activated nucleated particles (thin line) and equiaxed volume fraction (dotted line)

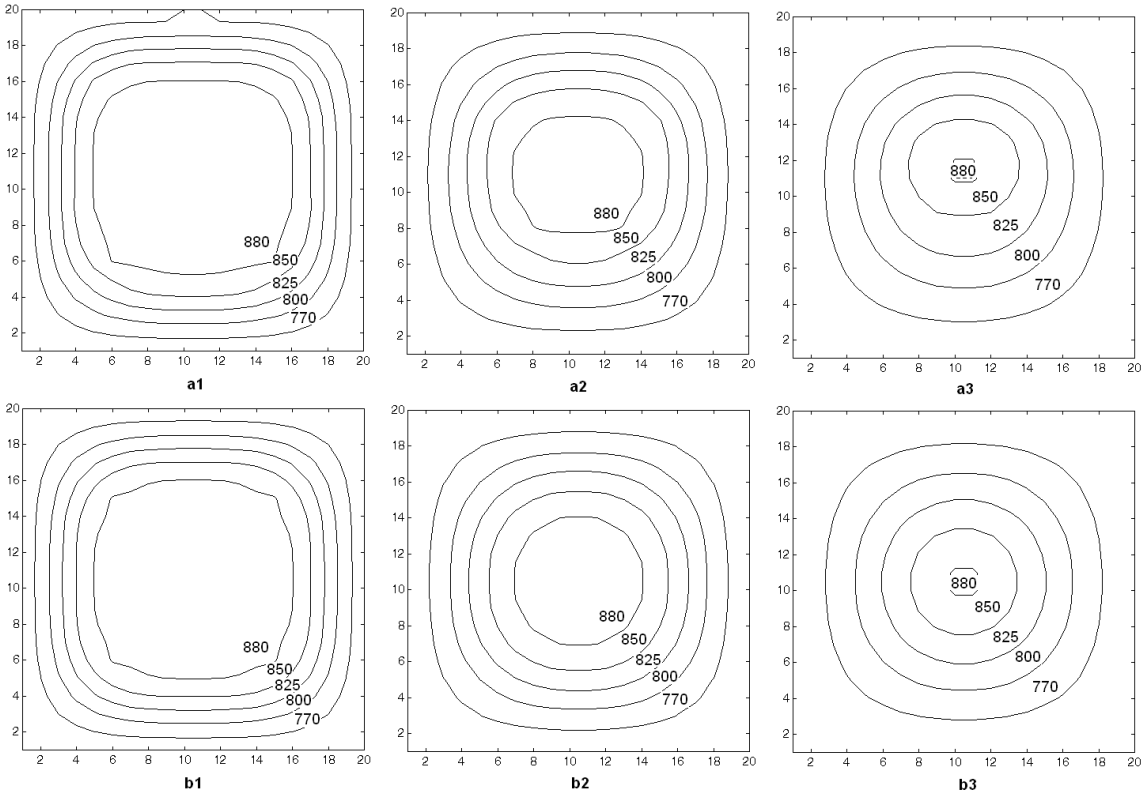

Figure 4. Simulated temperature contours during solidification with and with out convection (a1) 30 sec. - with convection (a2) 50 sec.- with convection (a1) 70 sec. - with convection (b1) 30 sec. – no convection (b2) 50 sec. - no convection (b3) 70 sec. – no convection

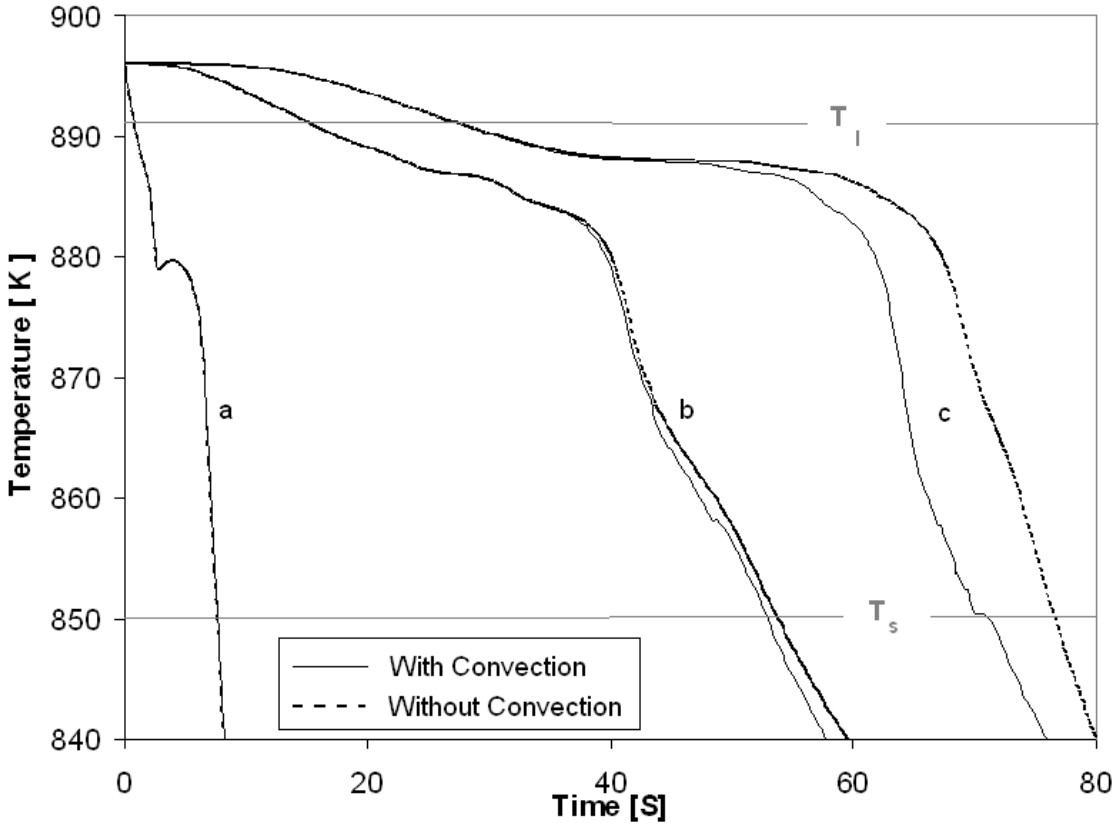

Figure 5. Cooling curves (a)close to the mould wall (b)half the way towards to the centre of the mould (c)centre of the mould

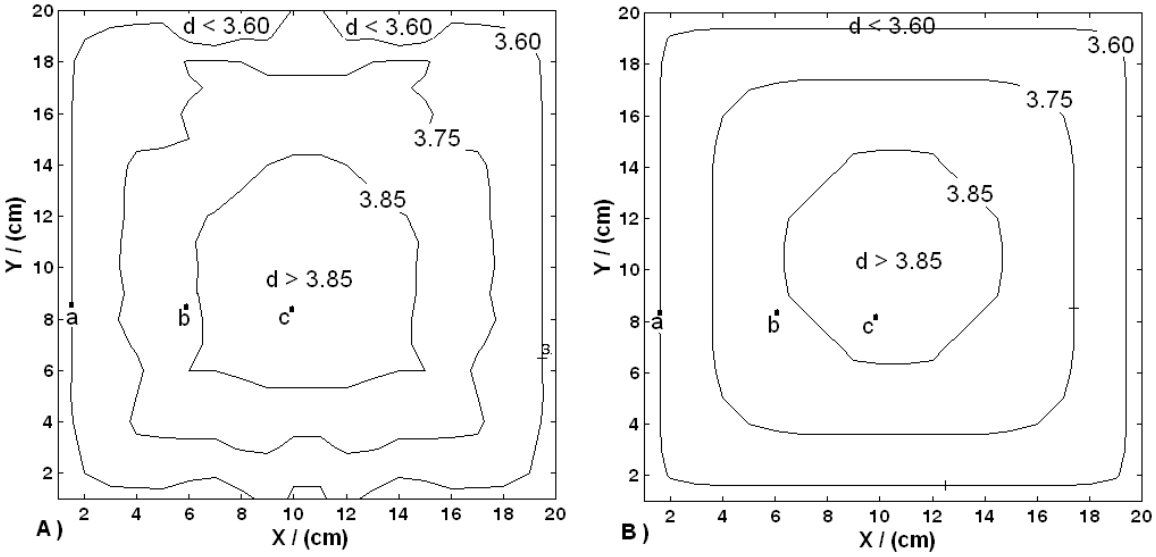

Figure 6. Grain size(diameter-*d*) distribution in millimetres A) with convective affects B) no-convection

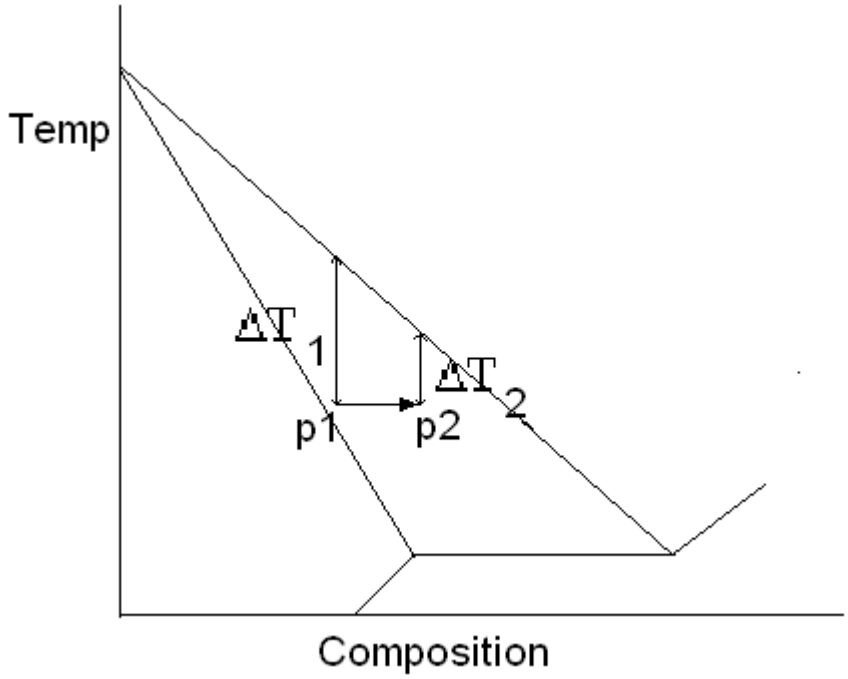

Figure 7. Shift of composition and reduced actual undercooling, in solute rich melt.